Research Square

Preprints are preliminary reports that have not undergone peer review.
They should not be considered conclusive, used to inform clinical practice,
or referenced by the media as validated information.

Geometric Guidelines for Estimating Fracture Toughness in Ductile Alloys Using Notched Cylinders

Larissa Simão
State University of Norte Fluminense
Rogerio Carvalho
Instituto Federal Fluminense
Francisco Rangel
Instituto Nacional de Tecnologia
Sergio Tavares
Fluminense Federal University
Eduardo Carvalho
eatem@uenf.br

State University of Norte Fluminense

Research Article

Keywords: Ductile Fracture, Triaxiality, Damage Mechanics, Finite Element Analysis, Notched Cylinder Model

Posted Date: June 12th, 2026

DOI: https://doi.org/10.21203/rs.3.rs-9839749/v1

License: This work is licensed under a Creative Commons Attribution 4.0 International License.
Read Full License

Additional Declarations: No competing interests reported.

Geometric Guidelines for Estimating Fracture Toughness in Ductile Alloys Using Notched Cylinders

Larissa Gomes Simão[a], Rogério Atem de Carvalho[b], Francisco Luiz Correa Rangel[c], Sérgio Souto Maior Tavares[d], Eduardo Atem de Carvalho[a*]

[a]Northern Fluminense State University (UENF), Advanced Materials Laboratory (LAMAV), Campos dos Goytacazes, RJ, Brazil;

[b]Innovation Hub/IFFluminense, Campos dos Goytacazes, RJ, Brazil/CPA/IA/SENAI CIMATEC, Salvador, BA, Brazil;

[c]National Institute of Technology, CENANO I, LH_2S, Rio de Janeiro, RJ, Brazil;

[d]Fluminense Federal University, TEM/UFF, Niterói, RJ, Brazil.

*eatem@uenf.br

Abstract

This article investigates the inverse correlation between the Triaxiality Index (η) and plastic fracture deformation (ε_f) in ductile materials. It argues that classic yield criteria, like von Mises, fail to predict final failure due to their insensitivity to hydrostatic stress. Using a notched cylinder under tension to simulate high triaxiality, 45 Finite Element Method (FEM) simulations were performed on AA 7075-T6 aluminum. The stress state was decomposed into a hydrostatic component (σ_m) promoting void growth, and a deviatoric component (σ_{vM}) governing yielding. Results show fracture initiates at the point of maximum triaxiality ahead of the notch, rather than at the maximum von Mises stress. This demonstrates that triaxiality primarily indicates internal damage; high hydrostatic tensile stress exponentially accelerates microvoid growth and reduces ductility. FEM simulations varying geometric ratios, notch depth (a/R) and root radius (R/ρ), identified an ideal fracture study range: $a/R \approx 0.50$ and $R/\rho \geq 30$. These geometries induce cleavage (or quasi-cleavage) without forming a plastic zone, which is crucial for reliably estimating fracture toughness (K_{Ic}) per ASTM E399 standards. Ultimately, triaxiality is the dominant metric for predicting failure initiation under high-strain conditions, making its analysis essential for mechanical

design safety. Comparisons with external experimental data confirm the Notched Cylinder Model (NCM) successfully estimates the K_{Ic} of ductile materials.

Keywords: Ductile Fracture, Triaxiality, Damage Mechanics, Finite Element Analysis, Notched Cylinder Model.

Nomenclature

η: Triaxiality Index (ratio of hydrostatic stress to von Mises stress).

σ_m: Hydrostatic or mean stress.

σ_{vM}: von Mises equivalent stress.

σ_1,σ_2,σ_3: Principal stresses.

σ_{nom}: Nominal stress (calculated using the nominal radius R).

σ_{net}: Net stress or stress in the resistant section (calculated using the resistant radius r).

σ_y: Yield strength.

σ_H: Hydrostatic stress (synonym for σ_m).

$\sigma_{f,c}$: Cleavage fracture stress.

τ: Shear stress.

p: Pressure (in hydrostatic compression context).

σ_r, σ_θ, σ_z: Normal stress components in cylindrical coordinates (radial, tangential, axial).

$\tau_{r\theta}$, τ_{xy}: Shear stress components.

σ_x, σ_y, σ_z: Normal stress components in Cartesian coordinates.

ϵ_f or **ε_f**: Equivalent plastic deformation/strain at fracture.

$\varepsilon_{(pl)}$: Accumulated plastic deformation.

ε_z: Strain in the z-direction.

a: Notch depth.

R: Radius of the nominal section of the cylinder.

ρ: Notch root radius.

r: Radius of the resistant section (ligament).

r_*: Non-dimensional radius (ratio of position x to total length r).

x: Position/distance from the origin.

θ: Angular coordinate.

$\mathbf{A_{nom}}$: Area of the nominal section.

$\mathbf{A_{net}}$: Area of the resistant (net) section.

$\mathbf{K_{Ic}}$: Plane-strain fracture toughness (Mode I).

$\mathbf{K_{I}}$: Stress Intensity Factor for Mode I opening.

E: Modulus of Elasticity.

v: Poisson's ratio.

$\mathbf{F_{rup}}$: Force at the moment of rupture.

$\mathbf{K_{tg}}$: Stress Concentration Factor relative to the nominal section.

$\mathbf{K_{tn}}$: Stress Concentration Factor relative to the resistant section.

$\mathbf{I_1}$: First invariant of the stress tensor (related to hydrostatic stress).

$\mathbf{J_2}$: Second invariant of the deviatoric tensor (related to von Mises stress).

$\mathbf{J_3}$: Third invariant of the deviatoric tensor.

θ or **Θ**: Lode angle.

ξ: Normalized Lode Parameter.

$\mathbf{s_i}$: Deviatoric principal stresses.

1. Introduction

The safety and durability of structures and mechanical components are pillars of modern engineering. The ability to accurately predict the behavior of materials under loading, especially in the regimes leading to failure, is therefore of paramount importance [2]. In metallic materials, ductile failure is a predominant failure type, characterized by substantial plastic deformation before final separation. Historically, Engineering has relied on yield criteria, such as those proposed by Tresca and von Mises, to determine the onset of plastic deformation. These criteria, based on maximum shear stress or distortion energy, are remarkably effective in predicting when a material begins to deform permanently. However, their applicability is limited [3].

They do not offer insights into the subsequent process of damage accumulation and eventual failure of the material at that point. The von Mises criterion, for example, posits that yielding is independent of hydrostatic stress, implying that a material subjected to pure hydrostatic pressure, however intense, would never yield, a prediction that contradicts

experimental observation [4]. Plastic deformation alone is not a sufficient indicator of failure. "Ductility," often treated as an intrinsic property of the material (measured, for example, by necking in a tensile test), is in fact not a constant. It is strongly influenced by the component's geometry and the nature of the applied loading [3]. Components containing notches, holes, or other geometric discontinuities exhibit a much lower overall deformation capacity than a smooth test specimen made of the same material.

This apparent contradiction is resolved by introducing the concept of stress state as a determining factor in fracture initiation. In this context, the dimensionless parameter known as the Triaxiality Index (η) emerges as the fundamental metric for quantifying this state. Triaxiality relates the hydrostatic component of stress, responsible for volume variation and internal "tension" of the material at the microscopic level, to the deviatoric (or shear) component, responsible for shape change and plastic flow.

For FEM simulation, AA 7075-T6 mechanical properties were used. While AA 7075-T6 is a ductile alloy, this study deliberately employs a Linear Elastic (LE) constitutive model to simulate the stress fields ahead of the notch. This approach is essential to identify the specific geometric limits where high stress triaxiality creates sufficient constraint to suppress macroscopic plasticity. By simulating the material in this limit state, we aim to define the precise geometric ratios (a/R and R/ρ) required to inhibit plastic flow, thereby allowing the determination of valid plane-strain Fracture Toughness (K_{Ic}) using reduced-scale cylindrical specimens.

The objective of this article is, therefore, to demonstrate and analyze the inverse correlation between the level of triaxiality at a point in a body and the elastic deformation present when the material fails at that point, for the situation of a notched cylinder containing an annular notch.

1.1. Stress State and Triaxiality

To understand the influence of triaxiality on deformation, it is essential first to decompose the stress state into its fundamental components and then connect these components to the physical

mechanisms that govern failure on a microscopic scale. Figure 1 summarizes this idea.

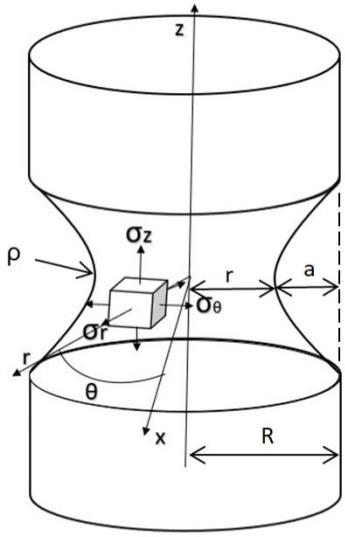


Fig1 Ring section of the studied cylinder, its dimensions and stress components. Adapted from [5]

1.1.1. Stress States and Stress Tensor Decomposition

Any stress state at a point can be described by a stress tensor, whose components can be obtained from this tensor, in particular for determining the three principal stresses: σ_1, σ_2, and σ_3. These components represent the normal stresses in planes where the shear stresses are zero. For the analysis of deformations and fracture, it is convenient to decompose this stress state into two parts with distinct physical meanings: a hydrostatic part and a deviatoric part [6].

The hydrostatic or mean stress (σ_m) is the arithmetic mean of the principal stresses and represents the uniform pressure or traction acting at the point. Mathematically, this average is expressed in the Equation 1:

$$\sigma_m = \frac{\sigma_1+\sigma_2+\sigma_3}{3} \quad (1)$$

A positive hydrostatic stress (tension) tends to cause volumetric expansion, while a negative one (compression) causes contraction. In the context of ductile failure, $\sigma_m > 0$ is the primary agent promoting the growth of internal microvoids, as will be discussed later. The von Mises equivalent

stress (σ_{vM}) (Equation 2), derived from the deviatory tensor, represents the magnitude of shear stress or distortion. It is the elastic distortion energy stored in the material and is the quantity that, according to von Mises' theory, governs the onset and continuation of plastic flow:

$$\sigma_{vM} = \sqrt{\frac{1}{2}[(\sigma_1 - \sigma_2)^2 + (\sigma_2 - \sigma_3)^2 + (\sigma_3 - \sigma_1)^2]} \quad (2)$$

In other words, while hydrostatic stress attempts to "open" the material, von Mises stress "deforms" it [7].

1.1.2. Triaxiality Index (η)

The triaxiality of stress, symbolized by η, is defined as the dimensionless ratio between the hydrostatic stress and the equivalent von Mises stress, as indicated in Equation 3:

$$\eta = \frac{\sigma_m}{\sigma_{vM}} \quad (3)$$

This parameter encapsulates the nature of the stress state. Different loading conditions result in characteristic values of η [8, 9]:

- **Uniaxial stress:** For a bar under simple tension ($\sigma_1 > 0$, $\sigma_2 = \sigma_3 = 0$), we have $\sigma_m = \sigma_1/3$ e $\sigma_{vM} = \sigma_1$, resulting in $\eta = 1/3$;
- **Uniaxial compression:** Similarly ($\sigma_1 < 0$, $\sigma_2 = \sigma_3 = 0$), this results in $\eta = -1/3$.
- **Pure shear:** In this case ($\sigma_1 = \tau$, $\sigma_2 = -\tau$, $\sigma_3 = 0$), the hydrostatic stress is zero ($\sigma_m = 0$), leading to $\eta = 0$;
- **Highly restricted states:** In regions such as the root of a notch or the front of a crack, plastic deformation is restricted in the transverse directions, generating tensile stresses in these directions. This raises the hydrostatic stress by a greater amount than the von Mises stress, resulting in high triaxiality ($\eta > 1/3$). In the particular case of the notched cylinder, $\eta \geq 1$;

- **Hydrostatic compression:** Under uniform pressure ($\sigma_1 = \sigma_2 = \sigma_3 = -p$), the von Mises stress is zero, and $\eta \rightarrow -\infty$. This state inhibits fracture and allows for immense plastic deformations, which is the principle behind processes such as hydrostatic extrusion.

1.2. Ductile Fracture Mechanisms: Void Nucleation, Growth, and Coalescence (VGC)

Failure in ductile metals is not an instantaneous event, but an evolutionary process that occurs at the microscopic level. This process, known as VGC, can be divided into three phases, as described by McClintock [10] and Rice & Tracey [11].

- **Nucleation:** Plastic deformation leads to deformation incompatibilities between the metal matrix and second-phase particles (inclusions, carbides, etc.). These high-stress interfaces become sites for the nucleation of small voids;
- **Growth:** Once nucleated, voids begin to grow as plastic deformation proceeds. This phase is most critically affected by the stress state. Analysis by Rice and Tracey [11] demonstrated that the growth rate of a void radius is exponentially dependent on hydrostatic stress. High hydrostatic tensile stress ($\sigma_m > 0$) acts as an internal pressure, expanding the void in all directions. Simultaneously, von Mises stress (σ_{vM}) deforms the surrounding matrix, causing the void to elongate in the direction of the highest principal stress;
- **Coalescence:** As deformation continues, voids grow and move closer to each other. Eventually, the material bond between adjacent voids becomes unstable, resulting in their union (coalescence). This event propagates rapidly, forming a macroscopic fracture surface.

High triaxiality (η) means that, for a given level of strain (σ_{vM}), there is a disproportionately large hydrostatic stress. This high σ_m dramatically accelerates the void growth phase. Consequently, voids reach the critical size for coalescence much faster, i.e., with a much lower level of

accumulated plastic deformation (ε_{pl}) in the matrix. This is the origin of the inverse correlation: the higher the triaxiality, the lower the deformation until fracture. Several studies [12, 13] have explored the effect of triaxiality and Lode angle on failure in ductile materials

1.2.1. Ductile Failure Locus

The ductility of a material is not a constant property, but rather a characteristic that depends critically on the stress state. To translate this dependence into a quantitative tool for design and analysis, the concept of the fracture locus (also known as the "fracture envelope" or "ductility curve") was developed [14].

The fracture locus is a two-dimensional diagram that represents the equivalent plastic deformation at fracture (ε_f) as a function of the present triaxiality (η) [15]. Each point on this diagram corresponds to a state of stress and strain under which the material fails. It is, essentially, a map of the material's ductile deformation capacity under different loading conditions [16].The fracture locus is typically determined experimentally through a series of mechanical tests with different specimen geometries, each designed to induce a distinct state of triaxiality in the critical region. Some common examples include [3]:

- **Smooth Uniaxial Specimen:** Produces $\eta \approx 1/3$. Provides the reference value for ductility in simple tension.
- **Notched Cylinders:** By varying the notch radius and the ratio between notch depth and the original section radius, a range of positive triaxialities can be generated, typically between $0.4 < \eta < 1.0$ or more [17].
- **Sharper notches** result in higher triaxialities.
- **Pure Shear Tests:** Geometries such as double-notched or butterfly specimens can induce $\eta \approx 0$.
- **Tensile Tests with Lateral Notches (Flat Notched Bars):** These can generate triaxialities in different regimes.

- **Compression/Tension Tests with Hydrostatic Pressure:** In specialized laboratories, by applying confining pressure, negative or very high triaxiality regimes can be explored.

For each test, the load and displacement are monitored until fracture. The triaxiality (η) in the critical region is calculated using analytical models (for simple geometries) or, more commonly and with greater accuracy, by Finite Element simulations that replicate the test [18]. The equivalent plastic strain accumulated at the fracture (ε_f) is then extracted at the same point of failure initiation in the simulation.

Characteristics and interpretation of the fracture locus according to Barsom & Rolf [19]:

- **Marked Decline:** The most prominent feature is the drastic decline in fracture strain (ε_f) as triaxiality (η) increases. This directly validates the inverse correlation discussed earlier: more restrictive stress states (with higher hydrostatic stress) severely limit the material's ability to deform plastically before fracturing.
- **Influence of Hydrostatic Stress:** For positive triaxialities, tensile hydrostatic stress promotes void growth, requiring less deformation to achieve coalescence. The larger η, the more efficient the void growth.
- **Negative Triaxiality Region (η < 0):** In this region, the hydrostatic stress is compressive. This means that the pressure attempts to "close" any existing voids or prevent their nucleation. Consequently, the ductility of the material increases dramatically. Under conditions of pure hydrostatic compression (where $\sigma_{vM} \rightarrow 0$ and $\eta \rightarrow -\infty$), the plastic deformation that a material can withstand before fracturing can be orders of magnitude greater than under tension.
- **Pure Shear Region (η = 0):** In this condition, hydrostatic stress is zero, and deformation is dominated by shear. Pure shear fracture often occurs through a mechanism of shear instability or elongated void coalescence, and ductility can be considerably high, although generally lower than in compression.

- **Material Characteristic Curve:** Each material has its own fracture locus. More ductile alloys will have a "higher" ε_f vs. η curve and possibly less steep in certain regions than less ductile materials. The locus can also be influenced by strain rate, temperature, and microstructure.

1.2.2. Von Mises Stress vs. Triaxiality

The region where fracture begins is determined by two main failure types [20]:

- **Ductile Failure (Plastic Yield):** Governed by Von Mises Stress (σ_{vM}) The material begins to deform plastically (yield) when σ_{vM} reaches the material's yield strength (σ_y);
- **Brittle Failure:** It is governed by Hydrostatic Stress (σ_H or σ_m) or by the maximum principal stress (σ_1). Triaxiality (η) is a direct indicator of this condition. High triaxiality means high hydrostatic stress.

Analysis of the frature surface indicates the presence of two distinct regions: the first being at the root of the notch ($r = 0$), where σ_{vM} is very high (maximum). However, $\eta = 0.52$ (relatively low). Thus, the biaxial stress state, typical of a surface, prevails. Therefore, this point marks the onset of plastic flow. If the material were to fail ductilely, failure (deformation) would start in this point, where the von Mises stress is highest. The other critical region is near the root of the notch ($r > 0$), where σ_{vM} is lower than at the root, but $\eta = 2.67$ (extremely high).

The high triaxiality (high hydrostatic stress) in this internal region has two effects: It suppresses plastic flow and promotes brittle fracture. In first case, even if there is stress, the high hydrostatic constriction locks the material, hindering the movement of dislocations and, therefore, flow, explaining why σ_{vM} is lower there. In second case, high hydrostatic stress pulls atoms apart, and, when the material’s nature allows, under specific conditions, it leads to cleavage as the failure mode. The absence of plasticity proves that the failure mechanism was not ductile (governed by

von Mises). Therefore, the fracture could not have started at the point of maximum σ_{vM} (at the root). The failure was, by definition, brittle. Brittle fracture begins where the condition for cleavage is first reached, i.e., at the point of maximum hydrostatic stress, which is indicated by the point of maximum triaxiality (η = 2.67). The rupture started just below the notch surface. This is characteristic behavior of brittle materials or ductile materials under high constriction (notched cylinder case), where brittle failure occurs internally before plastic (ductile) flow can start at the surface.

Thus, this study considers η_{max} and the stresses and strains acting at this point as the limit values for the failure of these geometries. Brittle failure becomes the dominant failure type when the cleavage condition is satisfied before or at the same instant as the yield condition. In fields of high plastic restriction, such as at the tip of a crack (where cleavage is most relevant), there is an approximate relationship between the maximum principal stress and the von Mises stress. For a work-hardened material, a reasonable approximation is that the maximum principal stress in the high triaxiality region is about 2.5 to 3 times the yield stress. This is verified in the cases presented by Simão [21] and summarized in Table 1.

Table 1
The value of the ratio between σ_1 and σ_{vM} (which in the limit is equal to σ_y) at the moment of failure, for three real cases, where no plastic deformation was observed after failure, using the notched cylinder and AA 7075-T6 aluminum alloy.

R/ρ	σ_1 at η_{max} (MPa)	σ_{vM} at η_{max} (MPa)	σ_1 / σ_{vM} at η_{max}
150.00	971.00	320.29	3.03
111.11	932.17	313.99	2.97
85.71	913.10	313.33	2.91

Cleavage becomes possible when the maximum principal stress that the stress field can generate ($\approx 3\sigma_y$) is equal to or greater than the cleavage fracture stress ($\sigma_{f,c}$). The ratio $\sigma_{f,c}/\sigma_y$ is the leading indicator. Aluminum alloys are not prone to cleavage failure, as this failure mode is rarely observed in such planes. However, experimental results indicate a phenomenon known as "quasi-cleavage," in which some regions of the fracture surface exhibit morphology similar to cleavage [5]. In cases where

cleavage does not occur, other microscopic evidence of brittle fracture is observed in regions where high hydrostatic stress suppresses plastic flow (governed by the Von Mises Stress, as previously mentioned).

1.2.3. Lode angle (θ)

The Lode angle (θ) is an azimuthal coordinate used to describe the shape of the deviatoric stress state at a specific point in a material. It provides crucial information about the relative combination of principal stresses and is widely used in yield and rupture criteria in soil and solid mechanics [22].

Geometrically, the total stress state at a point can be represented in a three-dimensional space of principal stresses (σ_1, σ_2, σ_3). The hydrostatic axis (s) is the line where $\sigma_1 = \sigma_2 = \sigma_3$. The plane perpendicular to this axis is called the deviatoric plane (or π plane). The Lode angle is the angle between a fixed reference axis in the deviatoric plane and the deviatoric stress vector in that plane. It defines the orientation of the stress state within the π plane, i.e., the "shape" of the deviatoric stress state.

To understand the Lode angle, it is useful to first classify the stress tensor (σ_{ij}) using its three invariants [23]:

- **Invariant 1 (I_1):** Related to hydrostatic stress (σ_m). It reflects how dilational the stress state is (tendency to expand or contract the volume).
- **Invariant 2 of the Deviatoric Tensor (J_2):** Related to von Mises equivalent stress (σ_{vM}). It measures the *magnitude* of distortion (change in shape), regardless of change in volume.
- **Invariant 3 of the Deviatoric Tensor (J_3):** This is the invariant used to define the Lode Angle. It describes the mode or type of distortion. $J_{(3)} = \det(s_{ij}) = s_1.s_2.s_3$, where $s_i = \sigma_i - \sigma_m$ are the deviatoric principal stresses.

1.2.3.1. Definition of the Lode Angle (Θ)

The Lode Angle, Θ, is defined mathematically by the relationship between J_2 and J_3 (Equation 4):

$$\cos(3\theta) = \frac{J_3}{\frac{2}{3}J_2^{3/2}} \quad (4)$$

In the common convention where the principal stresses are ordered ($\sigma_1 \geq \sigma_2 \geq \sigma_3$), the Lode angle varies within a limited range: $-30° \leq \theta \leq +30°$ due to the conventional ordering of the principal stresses ($\sigma_1 \geq \sigma_2 \geq \sigma_3$), which restricts the analysis to a specific sector known as the Haythornthwaite sector [24].

The limit values correspond to specific stress states:

- **Θ = -30°:** Corresponds to the state of pure triaxial compression ($\sigma_1 \geq \sigma_2 = \sigma_3$), where the intermediate principal stress is equal to the smallest principal stress;
- **θ = +30°:** Corresponds to the state of pure triaxial tension ($\sigma_1 = \sigma_2 > \sigma_3$), where the intermediate principal stress is equal to the largest principal stress;
- **θ = 0°:** Corresponds to a state of simple shear or balanced biaxial compression.

The physical significance of the angle of Lode lies in its ability to differentiate between stress states that have the same hydrostatic stress (I_1) and the same von Mises stress (J_2). It can be expressed by Lode Parameter, mathematically presented in Equation 5:

$$\xi = \frac{2\sigma_2 - \sigma_1 - \sigma_3}{\sigma_1 - \sigma_3} \quad (5)$$

It quantifies the "mode" of deviatoric loading. To facilitate interpretation, a normalized Lode Parameter (ξ) is often used, where ξ varies from -1 to +1 and has a very clear physical interpretation:

- **ξ = +1 (Θ = 30°):** Axial traction where the material is pulled along a main axis while being compressed equally on the other two (in the deviatoric plane);
- **ξ = 0 (Θ = 0):** The stress state is dominated by shear. The von Mises stress is equal to the maximum shear stress in the deviatoric plane. A classic example is the torsion of a shaft;
- **ξ = -1 (Θ = -30°):** Axisymmetric compression where the material is compressed along a principal axis while being equally tensile in the other two (in the deviatoric plane). Typically, the uniaxial compression test.

In summary, the Lode angle (or its parameter) tells us whether the state of distortion is closer to tension (ξ = 1, Θ = 30°), shear (ξ = 0, Θ = 0°) or compression (ξ = −1, Θ = −30°). The most critical application of the Lode angle is in ductile fracture modeling. Simple yield criteria, such as von Mises (J_2), ignore the Lode angle. They assume that the material yields at the same stress σ_{vM} regardless of whether it is tension, compression, or shear. In principal stress space, the von Mises yield surface is a cylinder whose radius depends only on J_2 .More advanced criteria (such as Drucker-Prager, Mohr-Coulomb, and many modern models for metals) include J_3 or the Lode angle [3, 25, 26, 27]. They recognize that most materials have different resistances to flow in tension, compression, and shear. Ductile rupture (by nucleation, growth, and coalescence of microvoids) is governed by two main parameters of the stress state: the triaxiality of stress η, which governs the growth rate of voids. High triaxiality accelerates void growth and reduces ductility. The other parameter is the Lode angle (ξ or Θ): It governs the shape of void growth and the coalescence mechanism. In tensile states (ξ ≈ 1), voids grow more spherically. In shear states (ξ ≈ 0), voids elongate and distort, leading to a void shearing failure mechanism, which generally occurs at much smaller plastic deformations [3].

1.3. Notched Cylinder

Hancock and Mackenzie recommended the cylindrical test specimen containing an annular notch, with ρ relatively large, which has been used since then [17] for studies of failure mechanisms in high-intensity triaxial states at the center of the resistant section. The use of the formulations made by Bridgman [4] is restricted to situations where the resistant section is fully plasticized and there is an area reduction (striction). Some authors point to the use of these expressions in cases where the test specimens have circular notches with ρ of the same order of magnitude as R [28, 29, 23]. In the case studied by Mackenzie, the authors state that failure initiates at the center of the test specimen, that is, in the region of maximum triaxiality, rather than at the point of greatest stress (at the notch root). The dimensions cited by the authors indicate that a/R = 0.50 and R/ρ = 1.2, 2, 3, 4, and 6. The finite element analysis performed by Simão (2024) [21] indicates that for these geometric relationships, we have approximately (Table 2).

Table 2
Ratio between stresses σ_{vM}, σ_1, σ_m, and σ_{nom} at the root of the notch, at the point where η is maximum, and at the center of the cylinder. Consider the dimensionless ratios a/R = 0.5 and R/ρ = 5.

	notch	**η_{max}**	**center**
σ_{vM}/σ_{nom}	6.86	1.35	1.35
σ_1/σ_{nom}	7.66	2.51	2.51
σ_m/σ_{nom}	3.25	1.61	1.61
H	0.47	1.20	1.20

It can be seen that although the elastic stress acting on the notch is about six times greater than that present at the center of the body, the failure starts at the center.

1.3.1. The Effect of Small ρ

This study, however, goes to the opposite extreme to that presented above, since it sought to examine combinations of a/R and R/ρ that yielded maximum triaxiality at a point near the notch root in the plane of the body's resistant section. This condition is dominant in the failure process, since when η_{max} is located at the center of the body, there is a possibility of plastic deformation forming as the crack propagates toward the notch root, thereby altering the stress distribution by reducing the hydrostatic component of the acting stress. The cylindrical geometry containing a ring, when R/ρ is greater than a given limit, prevents the formation of a plastic zone in the failed section of the cylinder. Thus, the rupture load values can be used in Tada's formulations [30] to estimate the correct K_{Ic} for that material.

Experimental evidences were presented by Simão [5] working with an AA 7075-T6 aluminum alloy. In aforementioned study, the author set a/R = 0.50 and varied R/ρ as shown in Table 3.

Table 3
Nominal stress at fracture of AA 7075-T6 notched cylinders and K_{Ic} calculated from these values and geometric characteristics.

R/ρ	P (mm)	σ_{nom} (failure) (MPa)	Formed Plastic Zone	K_{Ic} (MPa√m)
150.0	0.020	214.36	No	28
111.11	0.027	218.37	No	28
85.71	0.035	224.67	No	28
6.12	0.486	204.77	Yes	28
2.46	1.220	183.59	Yes	24
1.36	2.214	199.28	Yes	24

SEM analysis of the failed resistant sections and of higher R/ρ values (≈ 150, 111, and 86) showed that no plastic region formed at any point in the resistant section, indicating brittle fracture of the material. Interestingly, the R/ρ = 6.12 ratio yielded the correct fracture toughness, although it also showed some plasticized regions.

2. Materials and Methods

To apply the above postulates, a computational analysis using the Finite Element Method (FEA) was performed for a tensile test on a cylindrical test specimen with an annular notch. This geometry is ideal because it induces a triaxial stress state inside it. In order to analyze the stress field ahead of the notch, in the plane contained by the resistant section of the body and along the radius (r) of this section, see Figure 1, 45 simulations were generated, which employed the properties of the AA 7075-T6 aluminum alloy extracted from the tensile test with smooth test specimens [31, 21]. To simulate possible failure modes, two material models were assumed: Linear Elastic (LE) and Bi-Linear (BL). The choice of LE was based on the geometries sought not to generate a plastic region, and BL was chosen to simulate situations where a plastic zone was formed, in accordance with the provisions of the technical standard in Eurocode 9 [32]. The presence of a plastic zone was verified and measured by SEM analysis.

The exact determination of the stress components at the notch root is not possible using the Finite Element Method, since the more the mesh is refined, the higher the values obtained [33]. This study used meshes with quadrilateral axisymmetric elements, with 9 nodes per element and sides equivalent to 0.0056 mm (5.6 μm) in length, a value lower than those reported in other reviewed texts [34, 35]. Even with this limitation, given the level of mesh refinement, this study will assume that the values obtained are acceptable for their intended purposes.

The three main components of the stresses were determined, and from the equivalent stress (σ_{vM}) acting at the root of the notch, it was possible to estimate the Stress Concentration Factors for the nominal section (i.e., as a function of R), here referred to as K_{tg}, and those for the resistant section (as a function of r), i.e., K_{tn}. These factors were fundamental in equalizing the stress acting at the notch root for any geometric relationships among the used ones.

The FEM analysis was performed in two consecutive stages using the same meshes twice. In the first stage, the nominal stress was set to 100

MPa for all cases. This fixed value was used to simplify the calculation of the necessary K_{tg} and K_{tn}. In the subsequent stage, the nominal stress values are adjusted to produce the same stress magnitude in each model as that at which real test specimens failed. Thus, it is possible to adapt stresses greater or less than the reference stress to other geometries (a/R and R/ρ) (see Expression 6).

For the purposes of the calculations presented in this paper, the definitions of nominal stress (ρ_{nom}) and stress in the resistant section (ρ_{net}) are as follows:

$$\sigma_{nom} = \frac{F_{rup}}{\pi R^2} \quad (6)$$

Where F_{rup} is the force at the moment of specimen rupture and R is the radius of the nominal section of the cylinder (Equation 7).

$$\sigma_{net} = \frac{F_{rup}}{\pi r^2} \quad (7)$$

Where r is the radius of the resistant section of the cylinder.

And also, the non-dimensional r used throughout the text is the ratio between the position of the point where the measurement is reported (x) and the total length of the resistant section (r) (Equation 8):

$$r^* = \frac{x}{r} \quad (8)$$

For simulations performed in the second stage, values referring to actual test specimens, previously tested, were used, which presented R/ρ = 150 and a/R = 0.50. The nominal stress obtained in these tests, $\sigma_{nom,}$ was equal to 211 MPa, which refers to the average of the four values measured for these geometric conditions [21]. To verify the Fracture Toughness values obtained by the notched cylinder, ASTM E399 [1] and a CTS test specimen from the same plate from which the notched cylinders were manufactured and with the same rolling direction were used. Both tests presented a value of 28 MPa√m.

In order to impose the same level of stress acting at the root of the notch on all simulated geometries, Equation 9 was applied.

$$\sigma_{nom}^{exp}.K_{t_g-exp} = \sigma_{nom}^{MEF}.K_{t_g-MEF} \quad (9)$$

And the ratio between the nominal stress (R) and the stress acting on the resistant section (r) is expressed according to Equation 10:

$$\sigma_{nom} = \frac{\sigma_{nom}A_{nom}}{A_{net}} \quad (10)$$

Where A_{nom} is the resistant section of the region of radius R and A_{net} is that relative to the resistant section associated with r.

All simulated geometries considered geometrical ratios that are feasible in practice. Five notch depths were simulated (a/R = 0.25, 0.40, 0.50, 0.60, 0.75) in order to cover everything from shallow to deep notches. The radii of the notch root (ρ) simulated here followed the following proportions: R/ρ = 400, 200, 120, 60, 30, 20, 15, 7.5 and 5. This way, the ρ limit size to be machined with conventional techniques available was simulated [36]. For example, the ratio R/ρ = 400 is equivalent to a test piece following ASTM E8 [37] and with R = 3 mm → ρ = 0.0075 mm = 7.5 μm. Therefore, it is already considered difficult to manufacture by machining.

Once this was done, it was also possible to calculate K_{Ic} for each of these stresses [21], since it is not enough to fail without forming a plastic zone; it is also necessary to generate Fracture Toughness values equal to those predicted by the CTS test specimen.

2.1. Selection of Geometry and Mesh for FEM Analysis

The axissymmetric nature of the notched cylinder and the isotropy characteristic of metals such as aluminum alloys allowed only ¼ of its section to be simulated. This section represents a two-dimensional "slice" and its analysis is axisymmetric. Figure 2 shows this section. The elements used were 2D Axisymmetric Solids, with 9 nodes per element.

The geometric parameters indicated in item 3 are the most important characteristics of the test specimens, being decisive for the induced stress field and, therefore, the failure mode, to be as close as possible to that caused by a crack, where $\rho \rightarrow 0$. Finally, a notch flank angle of 60° was assumed, which was also tested by Simão [21] and fully met the desired requirements.

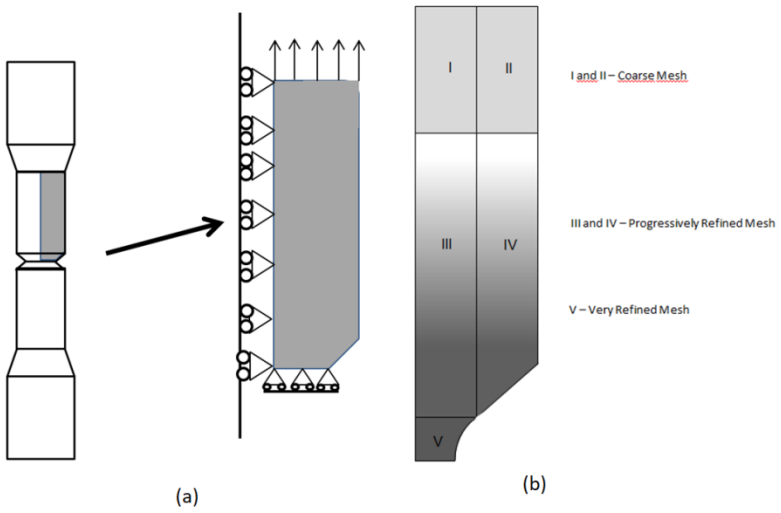


Fig2 Examples showing the section simulated (not to scale) by FEM with axisymmetric and 2D characteristics

2.2. Mesh Division and Refinement

The section studied has regions where stresses vary smoothly and others where the gradient is intense. To optimize the file sizes generated for processing, it was decided to divide the part into five regions with varying degrees of refinement. Figure 2b shows these regions and their refinement levels. Based on Figure 2 and considering I, II, IV, and V as the respective areas with different degrees of refinement, it is noted that the heights of III and IV were adjusted to represent 1/2 the length of the clip gage used in the actual tests (h/2 = 12.5 mm). Thus, the upper limit of these areas corresponds to the point at which the sensor contacts the test piece in the actual experiment, making the simulated cases as reliable as possible. Based on this decision, it is also possible to calibrate the clip gage measurement by MEF.

For comparison purposes, the refinement gradient was as follows: areas I and II had relatively low refinement, while III and IV had high refinement, and V had very high refinement. As already mentioned, 2D rectangular axisymmetric elements with nine nodes per element were used in this analysis. Considering the sharing of nodes across the common edges of each element, the meshes had, on average, 144,827 solid elements and 580,131 nodes. The two lines with the highest individual refinement were: the axis of symmetry representing half a resistant section (r) and the semi-arc at the bottom of the notch. This semi-arc was divided into 32 elements, or 64 nodes. Thus, each node was 0.000327 mm (= 0.327 μm) from its neighbors in the actual simulated case, where ρ = 0.02 mm.

The line from which the principal stress values are taken for the purpose of calculating the quantities of interest was divided into 1000 elements or 2000 nodes. For the case where a/R = 0.5 and R = 3 mm, the radius of the resistant section is 1.5 mm. Divided by 2000 equidistant nodes, the nodes are 0.000750 mm (= 0.75 μm) apart. This represents a degree of mesh refinement significantly higher than standard macroscopic fracture studies [15, 13], ensuring accurate capture of the steep stress gradients at the notch root. In simulated cases where ρ differed from the above, proportional adjustments (increasing the number of nodes) were made. This refinement was determined through an iterative process, considered "converged" when the difference between iterations was less than 0.1%. The mesh refinements were not identical, requiring adjustments for the different notch radii.

3. Results and Discussion

3.1. Triaxiality Levels

The following results, shown in Figure 3a-3e, represent the distribution of Triaxiality Index, η along the length r of the resistant section. Five depths were simulated: a/R = 0.25, 0.40, 0.50, 0.60, 0.75. At each notch depth, nine radii ρ were simulated, R/ρ = 5, 7.5, 15, 20, 30, 60, 120, 200, and 400. For illustration purposes, limits 1.0 and 2.0 were added. The

limit 1.0 represents the boundary where the average stress, σ_m, equals the von Mises stress, σ_{vM}. This would be the theoretical limit below which cleavage (or another brittle failure mode) will not occur. The limit 2.0 represents an average boundary above which cleavage occurs as a failure mode at a given point. (Check appendix A).

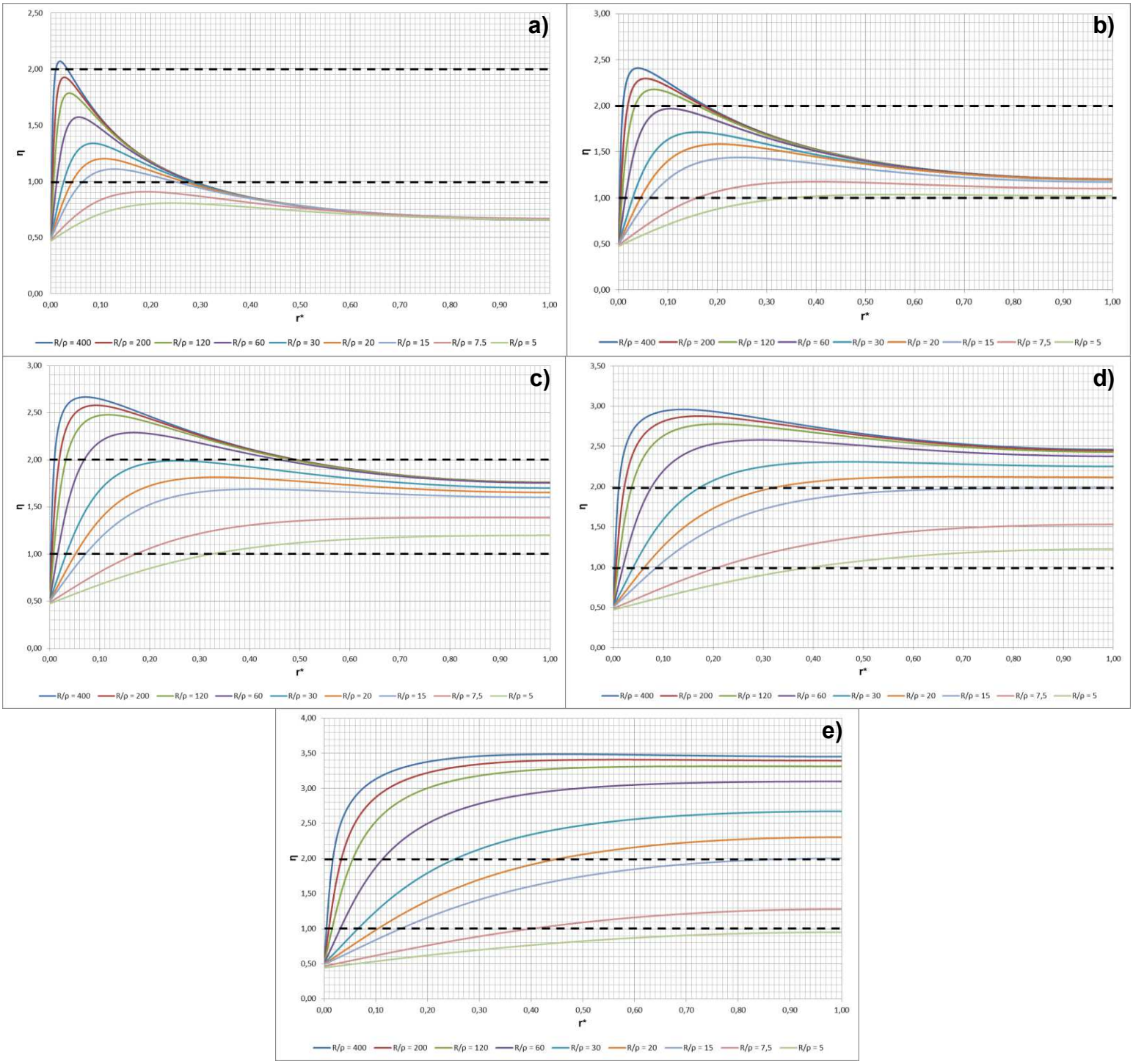


Fig3 Distribution of Triaxiality Index, η, along the length, r, of the resistant section. Where a/R = 0.25 **(a)**, 0.40 **(b)**, 0.50 **(c)**, 0.60 **(d)**, 0.75 **(e)**

The figures above indicate that the various geometries tested can be used to estimate the dimensions of test specimens capable of containing the stress levels and distribution required for various types of study. For example, if someone wants to induce failure very close to the notch root, he should select a depth $a/R = 0.25$ and $R/\rho = 400$. The fail will start very close to the notch, but with lower brittle failure probability than other cases with the same relative size of ρ, which implies the need for a higher nominal stress at fracture than in other cases (other a/R ratios), leading to an estimate of K_{Ic} greater than the actual value. For the case where one wishes to determine the Fracture Toughness of a given ductile material, the selection of a/R ratios that lie between the limits $0.40 \leq a/R \leq 0.60$ is the most convenient, since they balance the position where the maximum triaxiality is found, with its magnitude always greater than 2, ensuring cleavage, or another brittle failure mode, for small radii ($R/\rho \geq 120$). The ratio $a/R = 0.40$ produces the most pronounced peaks of η, but requires smaller radii ($R/\rho \geq 120$). At the other extreme, $a/R = 0.60$ presents a considerable region that is a candidate for initiating material failure, but it is tolerant of the size of ρ, which can be up to $R/\rho \geq 20$. The ratio $a/R = 0.50$ is the most balanced in these respects and is therefore the one that best reflects the quantity studied. This is consistent with the literature and technical standards [33, 1], which recommend that the ideal crack depth lies within the range $0.45 \leq a/R \leq 0.55$. Finally, $a/R = 0.75$ corresponds to the condition of a deep notch. For this ratio, the maximum value of η is found in the center of the test specimen. This situation is well explored by authors who wish to study the plastic region that forms before rupture [34, 35], associating it with large radii ($R/\rho \leq 60$). It can also be noted that the high triaxiality present implies a relatively lower nominal stress than for the other a/R ratios, which tends to yield a Fracture Toughness measurement, for example, lower than usual. Furthermore, this work considers that if failure occurs near the notch root and no plastic zone forms, the material suffered fracture. If the failure started at the center, what is being measured is the material's resistance to rupture.

3.2. *Ultimate Triaxility Index, η_{max}*

The ultimate value reached by η in each of the 45 geometries studied is shown graphically in Figure 4. It should be kept in mind that these values will occur in different locations for each simulated pair (a/R, R/ρ). The dashed lines represent the triaxiality value near the tip of the crack in an aluminum CTS (top line) and the lowest experimental value obtained using the notched cylinder (bottom line) for AA7075-T6.

3.2.1. *Reference Values*

There is no unique value to define a limit above which the triaxiality present at a point in the body imposes cleavage as the failure mode. However, it is possible to estimate a conservative limit by assuming that the magnitude of the triaxiality present in the region near the root of a crack is a reference value.

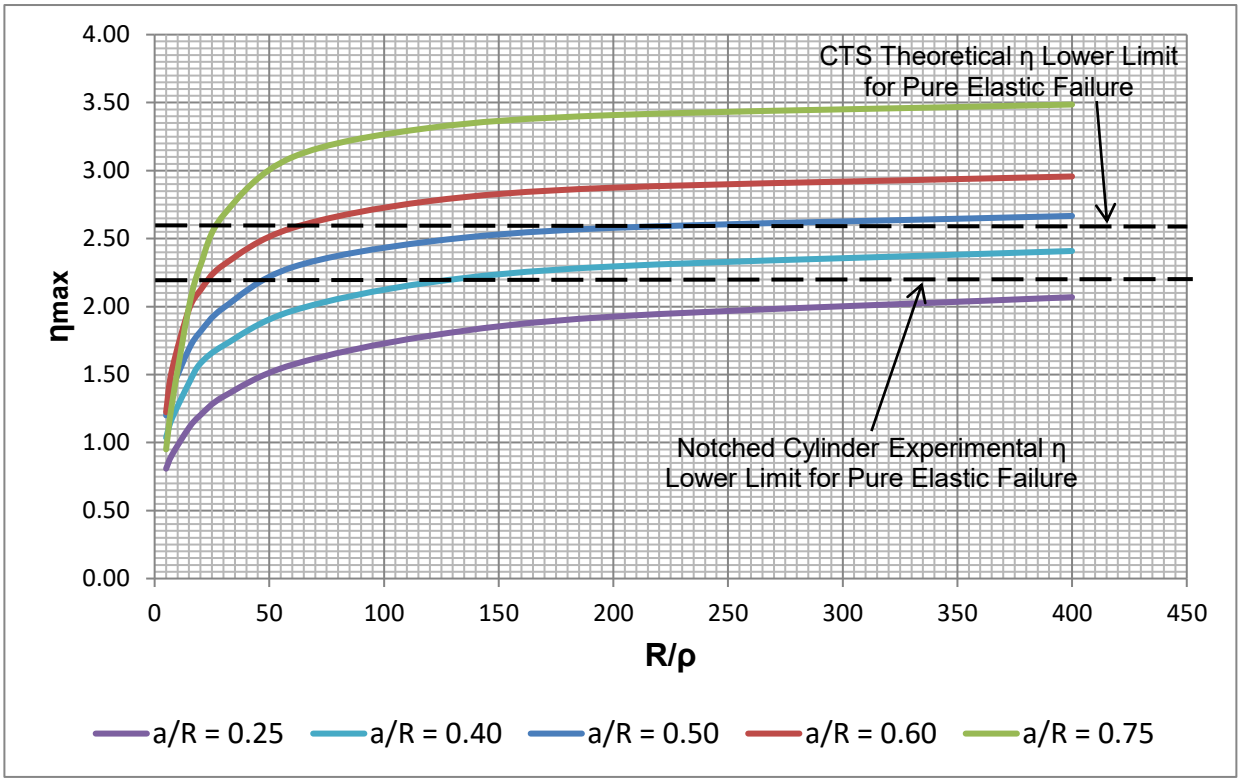


Fig4 Geometric parameterization for studies on fracture in AA 7075-T6 aluminum alloy. The values above the upper dashed line correspond to geometries that provide η above that obtained by the CTS

3.2.2. Estimation of η_{max} for a CTS Type Test Specimen – Crack and Notch

Appendix A presents the equations and deduction of the following expressions, where the stress field in the vicinity of a crack allows the value of η to be estimated for cases of a crack and a notch containing a radius, ρ, at its root. The first case (Equation 11) refers to the crack:

$$\eta_{max} = \frac{(2+2v)}{3\sqrt{(1-4v+4v^2)}} \quad (11)$$

Equation 11 indicates that in the region near the root of the crack and in the plane of the resistant section, the maximum triaxiality, expressed by η_{max}, is constant and depends only on Poisson's ratio.

Table 4 shows the values of η for some of the most common structural materials. These results were obtained by Equation 11:

Table 4
Values for Ultimate Triaxiality Index in the region near the crack tip, as calculated by Equation 11.

Material	Poisson's ratio	η_{max} (Equation 11)
Steel (carbon and alloys)	0.27 to 0.30	1.84 to 2.17
Stainless steel (austenitic)	0.27 to 0.31	1.84 to 2.30
Aluminum and alloys	0.32 to 0.34	2.44 to 2.79
Titanium and alloys	0.32 to 0.36	2.44 to 3.24
Copper and alloys (brass, bronze)	0.33 to 0.36	2.61 to 3.24
Cast iron	0.21 to 0.27	1.39 to 1.84
Nickel and alloys	0.28 to 0.31	1.94 to 2.30
Magnesium and alloys	0.29 to 0.35	2.05 to 3.00

Table 5 presents a comparison between the experimental results obtained with the notched cylinder ($R/\rho \geq 85$) and the predicted value for AA 7075-T6 aluminum alloy (for cracks) reported in the Table 4. Although the geometries are different (CTS x Notched Cylinder), it was assumed that,

regardless of the geometry of the body, cleavage will occur once similar levels of triaxiality are reached. The experimental results listed indicated the absence of a plastic zone in the resistant section after the fracture of the test specimen [5]. The values of η_{max} were determined using FEM and the mechanical properties measured during the tests.

Consultation of Table 4 indicates that there is no universal minimum value for the Triaxiality Index that imposes cleavage as a failure mode on any ductile structural material. Table 4 can, however, serve as a reference, understanding that the values listed are conservative, as shown in Table 5.

The second case studied presents the case of a non-singular notch. The stress field in the vicinity of the notch root with radius, ρ, generates the expression for estimating triaxiality (Equation 12):

Table 5
Ultimate Triaxiality Index in three real cases, using the Notched Cylinder Model in AA 7075-T6 aluminum alloy.

R/ρ	η_{max} (Notched Cylinder)	η_{max} (CTS)	Δ% (CTS x Notched Cylinder)
150.0	2.39	2.61	8.4
111.11	2.32		11.11
85.71	2.26		13.41

$$\eta_{max} = \frac{(2+2v)}{3\sqrt{\frac{3\rho^2}{4r^2}+(1-2v)^2}} \quad (12)$$

Equation 12 indicates that in the region near the notch root and in the plane of the resistant section, the maximum triaxiality intensity, expressed by η_{max}, is dependent on Poisson's ratio, the notch root radius, ρ, and resistant section radius, r. Equation 12 produces the same results to 11 up to the limit of R/ρ = 60. These values refer, again, to the case of CTS.

3.3. Deformations and Triaxiality

As expected, in regions of higher triaxiality, there is a lower level of deformation than at the notch root. For experimental cases with no plastic

deformation, the stress of interest in the η_{max} region is σ_1, as explained above. Figure 5 shows the ratios of the deformation at the point of maximum η to the equivalent deformation acting on the resisting section. This theoretical deformation corresponds to the nominal stress converted to the resistant section (see Equation 6), divided by the modulus of elasticity, E. This figure shows that the greater the notch depth, the lower the deformation at the point of maximum triaxiality at failure. Moreover, for average depths, the ratio of deformations at η_{max} reaches 0.4. This value is fixed for any level of elastic stresses applied to the body, since both deformations depend equally on the applied load. For notches ranging from medium to deep, the ratio between deformations tends to be constant for small ρ.

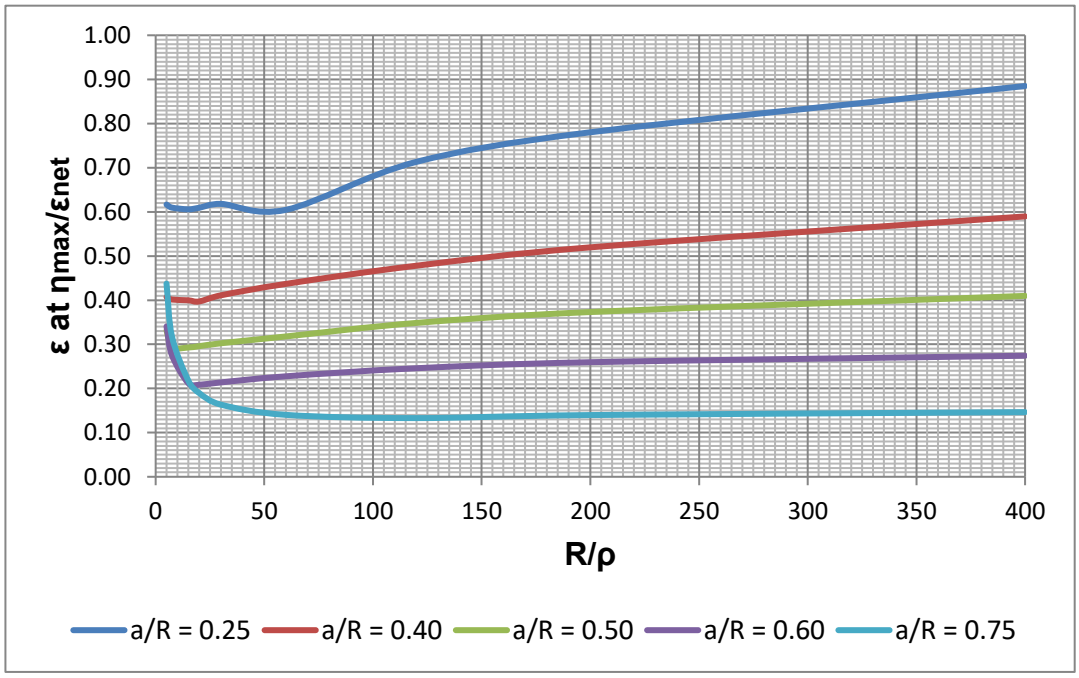


Fig5 Ratio between the deformation acting at point η_{max} and the net deformation

Figure 6 shows the ratio between the deformation at the center of the body and the nominal deformation, which is calculated based on the nominal deformation at the cross section (Eq. 7). For a depth of a/R = 0.75, the ratio becomes constant and equal to 2 from R/ρ ≥ 130. For depth a/R = 0.60, the ratio becomes equal to 1 after R/ρ ≥ 100. And for the remaining depths, there is agreement and convergence to 0.90 from R/ρ ≥ 30.

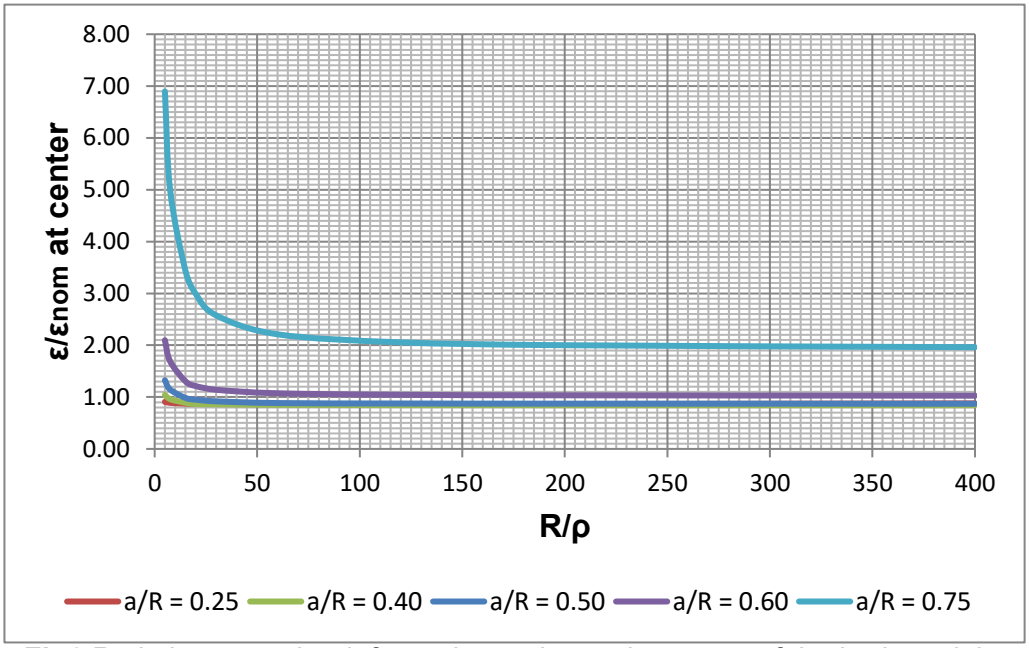


Fig6 Ratio between the deformation acting at the center of the body and the nominal deformation

Figure 7 shows the ratios of the highest principal stress (σ_1) measured at point η_{max} to the nominal stress. It can be seen that the greater the notch depth, the greater the stress ratio, in agreement with the results shown in Figures 5A-E. This geometry requires proportionally less nominal stress to break (even when corrected for variation in the resistant section), leading to lower fracture parameter than those of the other geometries. On the other hand, the shallowest notch has the lowest ratio, reiterating the observation that shallow notches require proportionally higher stress to rupture, which induces K_{Ic} to be higher than that obtained at greater depths.

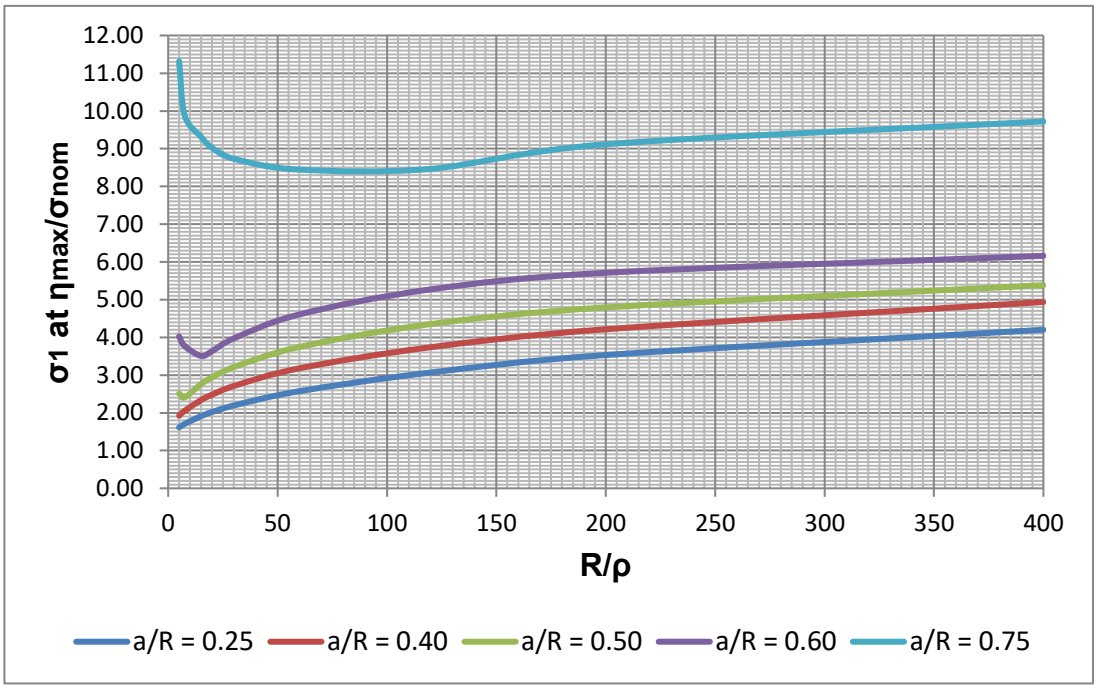


Fig7 Ratio between $\sigma_1$and σ_{nom} at the points of η_{max}

Figure 8 shows the ratio of the principal stress (σ_1) measured at the point of η_{max} to the stress acting on the resisting section (σ_{net}), as a function of η_{max}. In this case, the shallowest notch (a/R = 0.25) has the highest stress ratio. Using the resistant section as a reference reverses the results of the previous item. However, they remain fully compatible, since the nominal stress is constant across all simulations, whereas the net stress in the resistant section varies with area.

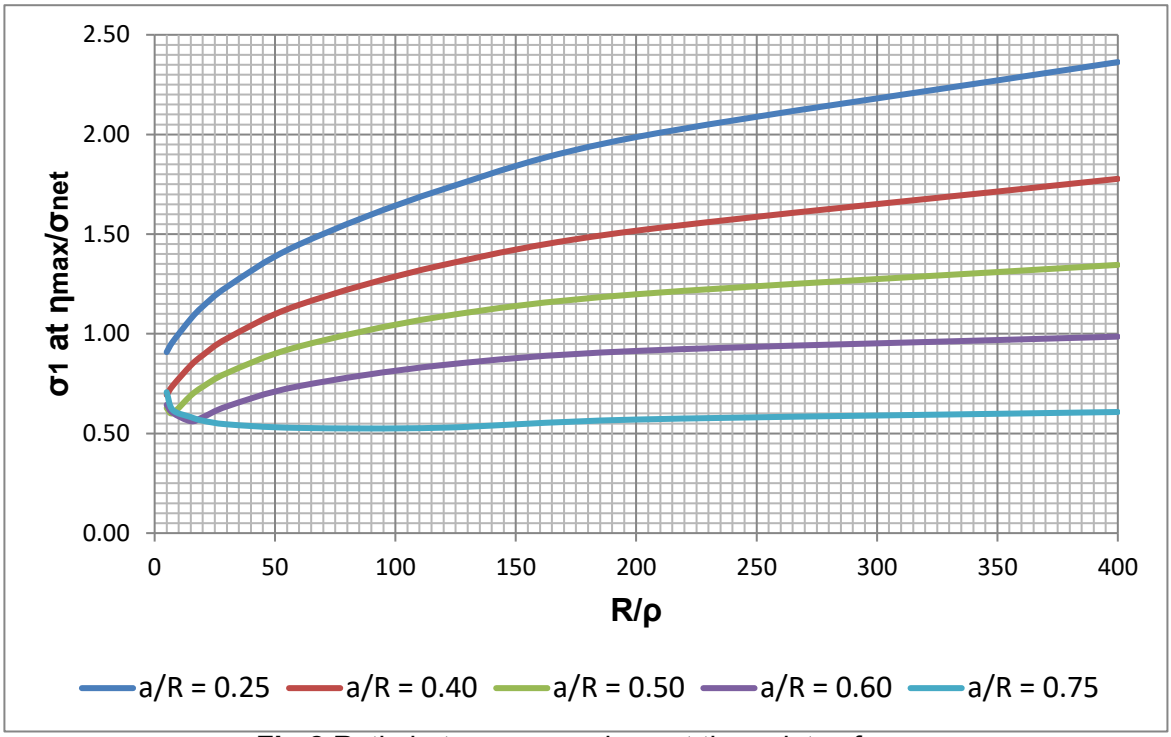


Fig.8 Ratio between σ_1 and σ_{net} at the points of η_{max}

3.4. Triaxiality and Lode Parameter

It was observed that for all simulations performed, the maximum value for the Lode parameter (ξ) was one and always located at the center of the body. The magnitude of this parameter varied by no more than 15% for the values obtained for the point where triaxiality is maximum. For values of $a/R \leq 0.60$, there is an inverse relationship between the depth of the notch and the values of ξ at the point where η is maximum for values greater than R/ρ. For values of R/ρ in the region $5 \leq R/\rho \leq 30$, this value tends towards unity, which indicates that for ρ, there is a greater probability of flow. The reverse is observed for smaller ρ.

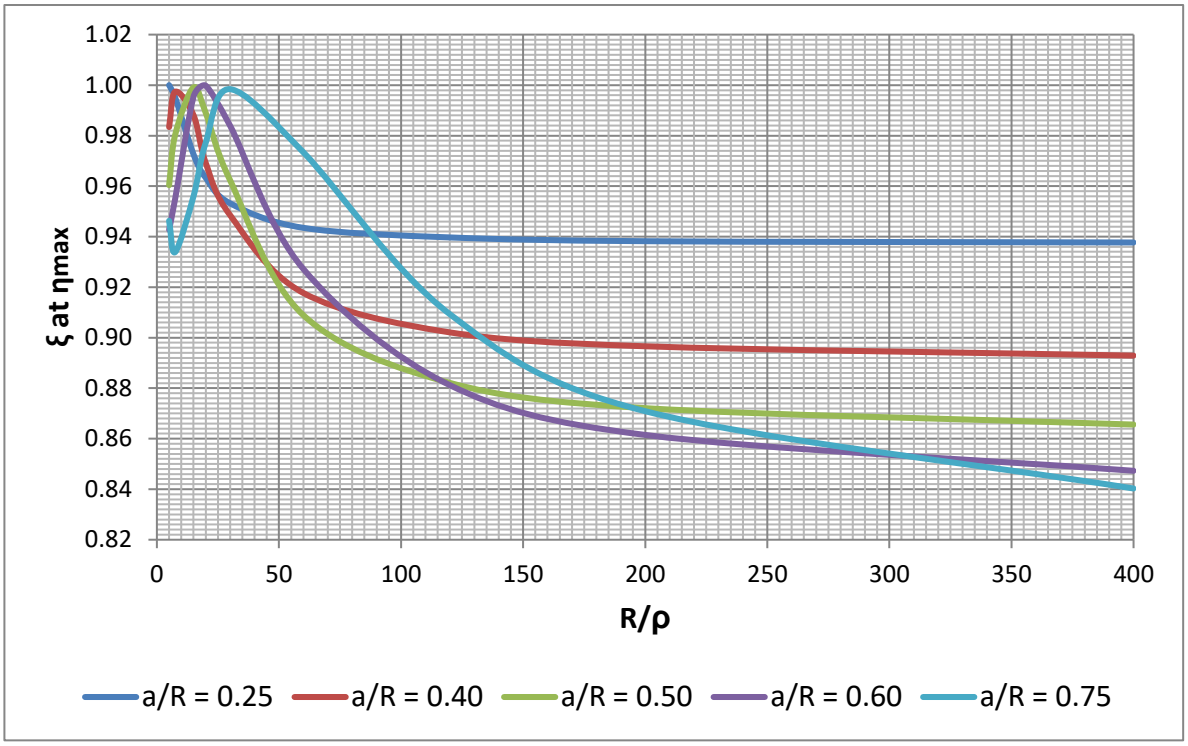


Fig9 Relationship between the relative size of ρ and ξ observed at the points of maximum η, for the various notch depths studied

3.5. Distance of η_{max} from the notch root

Figure 10 shows the curves generated from the position of each value of η_{max} for the cases analyzed. It should be noted that a value close to zero indicates that the maximum triaxiality is close to the notch root, which is the region that favors the measurement of Fracture Toughness. At the opposite extreme, when the dimensionless radius (r*) approaches unity, it indicates a geometry that will cause material failure in the central region, not lending itself to fracture studies. As shown in Figure 5A, the shallowest notch depth (a/R = 0.25) offers the positions of η_{max} closest to the root of the notch. The depth equivalent to a/R = 0.40 provides reasonable proximity and does not exhibit maximum triaxiality at the center of the cylinder in any of the cases studied. The average depth a/R = 0.50 presents η_{max} far from the center up to R/ρ ≥ 30. For the depth a/R = 0.60, this limit is R/ρ ≥ 120. Finally, for really deep notches (a/R = 0.75), η_{max} is already located at the center of the dimensionless resistant section radius (r*), close to the middle. For lower R/ρ values, the point where triaxiality is highest is clearly at the center. This justifies the choice of several authors, already mentioned

above, for large ρ and also considerable notch depth. Failure in these cases will start at the center, probably after the resistant section has completely yielded.

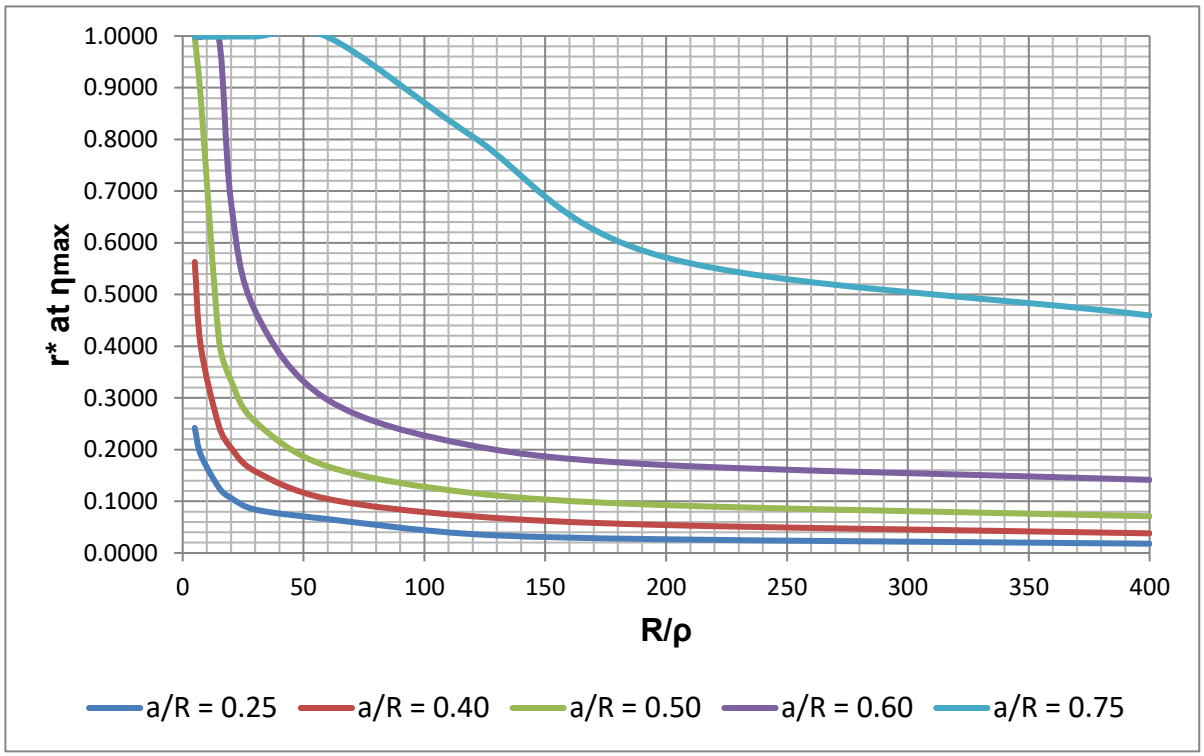


Fig10 Distance measured from the root of the notch where η_{max} occurs

3.6. The Validity of the Linear Elastic (LE) Assumption for the AA 7075-T6 Alloy

The validity of the Linear Elastic (LE) assumption for the AA 7075-T6 alloy, typically considered ductile, is justified by the specific stress state induced by the selected notch geometries. The Finite Element Analysis demonstrates that for sharp notches ($R/\rho \geq 30$), the Triaxiality Index (η) exceeds 2.0 in the critical region.

Physically, this high triaxiality represents a dominance of hydrostatic tension (σ_m) over the von Mises deviatoric stress (σ_{vM}). While σ_{vM} drives dislocation motion and plastic flow, high hydrostatic tension restricts volumetric change and effectively locks the material crystal lattice, inhibiting the onset of yield even at high load levels. Under these high-constraint conditions, typical brittle failure mechanisms are observed, even locally, before the yield criterion is satisfied: tongues and cleavage facets coexisting

with dimples (quasi-cleavage) [5, 38]. In addition, other microscopic features can be observed, such as a reduction in the size and number of dimples (more common in CFC metal alloys) (Figures 11 and 12a). Transgranular fracture originating from second-phase particles rich in Fe, Cu, Si, and Al (which are more brittle than the aluminum matrix [5]) was observed even in cases where the notches were larger. This is because the presence of the intermetallic compound breaking in a brittle manner does not preclude the dimple Nucleation-Growth-Coalescence phenomenon, which predicts that, depending on the size of the microvoids, once coalesced, they become potential defects that, by propagating across the grains, can lead the material to failure (Figure 13).

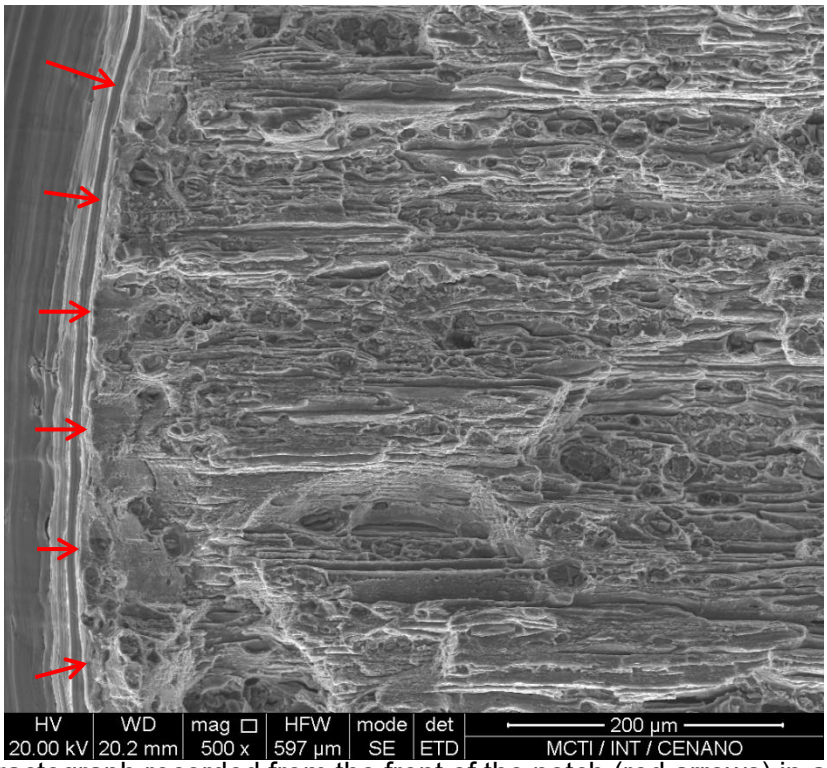


Fig11 Fractograph recorded from the front of the notch (red arrows) in a cylinder with V-notch and ρ = 0.030 mm (R/ρ = 86) no evidence of a plastic zone. 500x magnification

SEM analysis of the resistant sections for high-constraint specimens (R/ρ ≈ 86 − 150) revealed no evidence of a plastic zone (Figure 11). This is most evident when comparing the fracture surface of a cylinder with a V-notch of 0.025 mm radius (Figure 12a) to that of a test specimen with a U-notch of 1 mm radius. Figure 12b shows evidence of a plastic zone for the U-notch case, as indicated by shear lip. Consequently, employing an

elastoplastic material model in this specific regime would be methodologically incorrect, as it would artificially predict a plastic zone size and stress redistribution that does not physically occur. Therefore, the Linear Elastic model provides the most accurate representation of the stress field at the moment of failure for these specific high-triaxiality geometries.

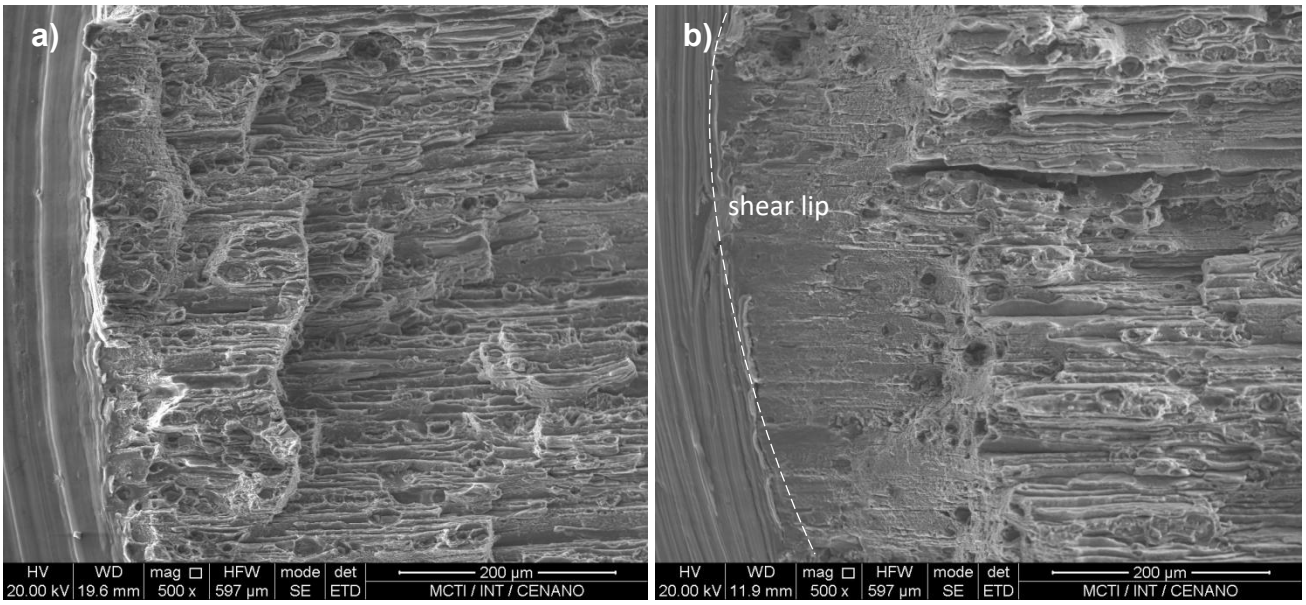


Fig12 Comparison of fractographs without and with evidence of a plastic zone: (a) V-notch of 0.025 mm radius (R/ρ = 111) and (b) U-notch of 1 mm radius (R/ρ = 6). 500x magnification

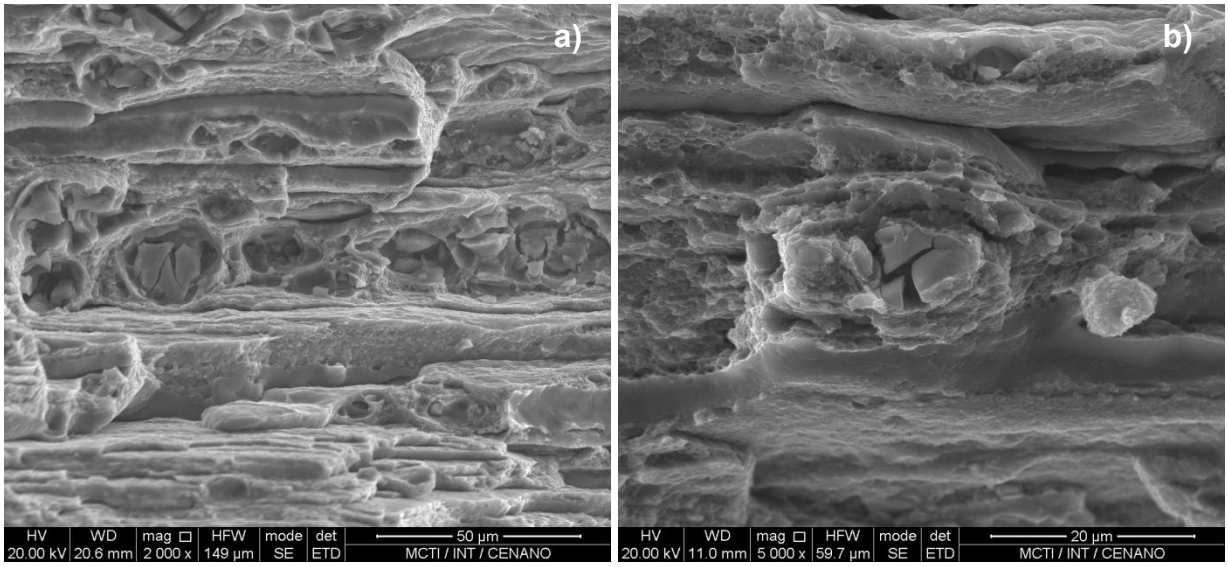


Fig13 Intermetallic particles acting as stress concentration sites. (a) U-notch of 0.49 mm radius (R/ρ = 6.12) and (b) U-notch of 1.22 mm radius (R/ρ = 2.46). 2000x and 5000 x magnification, respectively

3.7. Triaxiality Effect on Fracture Toughness

The compilation of experimental results and numerical simulations indicates that failure initiates at the point of greatest triaxiality. The K_{Ic} calculated from the results obtained by FEM indicated that the geometric ratios that most favor obtaining results equal to those obtained by using CTS are described in Figure 4. Cross-referencing this information with that presented in Figure 5, we can exclude geometries whose η_{max} is located at the center of the body, since this condition does not guarantee cleavage. Therefore, the optimal range for use is as described in Table 6. The limit of 2.0 was chosen based on the theoretical estimates and experimental results described here.

Table 6
Ratios most favorable to obtaining cleavage as the mode of failure.

a/R	R/ρ
0.40	≥ 120
0.50	≥ 30
0.60	≥ 60

It can be noted that the ratio a/R = 0.50 is the most flexible and tolerant, which supports its choice for studies aimed at estimating Fracture Toughness. The curves described in Figure 5 also allow to determine the region of the test specimen where cleavage (or quasi-cleavage) most likely began. Figure 14 illustrates this point.

This delimits the region of study via SEM, reducing the time and costs of the work, as presented and extensively discussed by Simão [5].

Table 7 shows the K_{Ic} values obtained from tests on actual specimens compared with those predicted by the CTS.

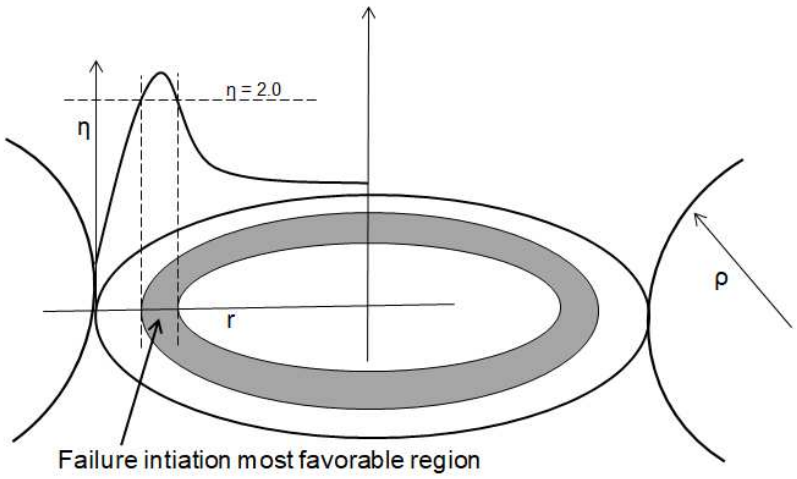


Fig14 Region of the test specimen where cleavage (or quasi-cleavage) most likely initiated

Table 7
K_{Ic} values obtained from tests on actual specimens compared with those predicted by the CTS.

R/ρ	K_{Ic} – Notched Cylinder (MPa√m)	K_{Ic} – CTS (MPa√m)	ΔK_{Ic} % (CTS x Notched Cylinder)
150.0	27.77	28.43	2.32
111.11	27.98		1.58
85.71	28.23		0.70

4. Conclusions

This study investigated the inverse correlation between stress triaxiality and fracture strain in ductile materials, establishing the Notched Cylinder Model (NCM) as a robust tool for estimating Fracture Toughness (K_{Ic}). By simulating high-constraint states in AA 7075-T6 alloy, the following conclusions are drawn:

- **Triaxiality as the Dominant Failure Driver:** The dissociation between the location of maximum von Mises stress (notch root) and maximum triaxiality (sub-surface) confirms that failure is driven by hydrostatic tension rather than shear distortion. Fracture initiates at the point of maximum triaxiality (η_{max}), where microvoid growth is

exponentially accelerated, rather than at the point of maximum plastic strain.

- **Validity of the Linear Elastic (LE) Model:** A critical methodological finding is that for sharp notch geometries ($R/\rho \geq 30$), the high hydrostatic constraint ($\eta > 2.0$) effectively suppresses the formation of a macroscopic plastic zone. Consequently, the material fails via a peculiar mode (quasi-cleavage) or by cleavage (if the nature of the material allows it) before satisfying the yield criterion. In this specific regime, employing a Linear Elastic constitutive model provides a more physically accurate representation of the failure state than elastoplastic models, which would predict a plastic zone that does not experimentally exist.
- **Optimal Geometric Parameters:** To reliably estimate K_{Ic} using a cylindrical specimen, the geometry must induce a Triaxiality Index sufficient to trigger brittle failure. The results indicate that:
    - *Optimal Range:* The ratios $a/R \approx 0.50$ and $R/\rho \geq 30$ provide the most reliable convergence with standard Compact Tension Specimen (CTS) results.
    - *Notch Depth Effects:* Shallow notches ($a/R < 0.40$) result in lower η_{max} peaks, artificially inflating fracture stress requirements. Conversely, deep notches ($a/R > 0.60$) shift the failure initiation point toward the center of the specimen, which is less representative of crack-tip fields.
- **Threshold for Brittle Failure:** While there is no universal triaxiality limit for all ductile materials, this study suggests a conservative reference value of $\eta \approx 2.0$ for aluminum alloys. Experimental fractography (SEM) validated the numerical predictions.
- **Role of Lode Angle:** The analysis indicates that for these axisymmetric geometries, the Lode parameter remains nearly constant in the high-triaxiality region. This confirms that for the specific purpose of K_{Ic} estimation in round bars, the Lode angle is a secondary variable, and triaxiality is the primary governing parameter for failure.

In summary, the Notched Cylinder, when designed within the geometric limits established in this work, offers a rapid and cost-effective alternative to standard CTS testing, providing accurate Fracture Toughness estimates for ductile alloys by geometrically inducing a brittle failure mode.

Acknowledgments

The authors would like to thank CAPES for publication support, and UENF (State University of Norte Fluminense) for the PAPIC funding (Edital PROPPG 5/2024) and CENANO/INT – National Institute of Technology, for the SEM analysis and support.

Declaration of generative AI and AI-assisted technologies in the manuscript preparation process

During the preparation of this work the author(s) used Grammarly in order to review the proper use of the English language and Gemini for initial paper review and figure numbering check. After using these tools, the author(s) reviewed and edited the content as needed and take(s) full responsibility for the content of the published article.

References

[1] American Society for Testing and Materials. Standard Test Method for Linear-Elastic Plane-Strain Fracture Toughness of Metallic Materials: E399-22 (2022) United States;

[2] Castro JTP, Meggiolaro MA (2009) Fadiga: Técnicas e Práticas de Dimensionamento Estrutural sob Cargas Reais de Serviço. 1st ed. Vol. 1. Create Space, Estados Unidos;

[3] Bai Y, Wierzbicki T (2008) A new model of metal plasticity and fracture with pressure and Lode angle dependent state. International Journal of Plasticity 24(6): 1071-1096.
https://doi.org/10.1016/j.ijplas.2007.09.004

[4] Bridgman PW (1952) Studies in Large Plastic Flow and Fracture with Special Emphasis on the Effects of Hydrostatic Pressure. 1st ed. McGraw-Hill, New York;

[5] Simão LG, Terrones LAH, Rangel FLC, Carvalho EA (2025) Fractographic analysis in the light of the triaxiality index of cylindrical specimens simulating fracture or rupture failures. Engineering Failure Analysis 178: 1-24.
10.1016/j.engfailanal.2025.109681

[6] Malvern LE (1969) Introduction to the Mechanics of a Continuous Medium. Prentice-Hall;

[7] Zhou J, Gardner L (2025) New void growth-based ductile fracture models incorporating interaction effects of stress triaxiality and Lode angle parameter. Theoretical and Applied Fracture Mechanics 140: 105204.
10.1016/j.tafmec.2025.105204

[8] Peng Z, Zhao H, Li X (2021) New ductile fracture model for fracture prediction ranging from negative to high stress triaxiality. International Journal of Plasticity 145: 103057.
https://doi.org/10.1016/j.ijplas.2021.103057

[9] Li T (2017) Fracture strain of gun steel for ultra-high-pressure vessels considering triaxiality effect. Advances in Mechanical Engineering 9 (11): 1-13.
https://doi.org/10.1177/168781401771497

[10] McClintock FA (1968) A criterion for ductile fracture by growth of holes. ASME Journal of Applied Mechanics 35: 363-371.
https://doi.org/10.1115/1.3601204

[11] Rice JR, Tracey DM (1969) On the ductile enlargement of voids in triaxial stress fields. J. Mech. Phys. Solids 17: 201-217.
10.1016/0022-5096(69)90033-7

[12] Peng J, Zhou P, Wang Y, Dai Q, Knowles D. Mostafavi, M (2021) Stress Triaxiality and Lode Angle Parameter Characterization of Flat Metal Specimen with Inclined Notch. Metals 11: 1-14.
https://doi.org/10.3390/met11101627

[13] Liu X, Yan S, Rasmussen KJR, Deierlein GG (2022) Experimental Investigation of the Effect of Lode Angle on Fracture Initiation of Steels. Engineering Fracture Mechanics 271: 108637.
10.1016/j.engfracmech.2022.108637

[14] Bao Y, Wierzbicki T (2004) On fracture locus in the equivalent strain and stress triaxiality space. International Journal of Mechanical Sciences 46(1): 81-98.
https://doi.org/10.1016/j.ijmecsci.2004.02.006

[15] Jones M, Hole M, Davies CM (2020) A Comparison of Stress Triaxiality and Strain Distributions in Notched Bar Geometries as Determined by Bridgman Expressions and Finite Element Analysis. Procedia Structural Integrity 28: 2078-2085.
https://doi.org/10.1016/j.prostr.2020.11.032

[16] Li W, Liao F, Zhou T, Askes H (2016) Ductile fracture of Q460 steel: Effects of stress triaxiality and Lode angle. Journal of Constructional Steel Research 123: 1–17.
https://doi.org/10.1016/j.jcsr.2016.04.018

[17] Hancock JW, Mackenzie AC (1976) On the mechanisms of ductile failure in high-strength steels subjected to multi-axial states of stress. Journal of the Mechanics and Physics of Solids 24(2-3): 147-160.
10.1016/0022-5096(76)90024-7

[18] Jeong W, Kim C, Li C-A., Bong HJ, Hong S-H, Lee M-G (2022) A probabilistic mean-field and microstructure based finite element modeling

for predicting mechanical and ductile fracture behavior of the cast aluminum alloy. International Journal of Plasticity 154: 103299. https://doi.org/10.1016/j.ijplas.2022.103299

[19] Barsom JM, Rolfe ST (1999) Fracture and Fatigue Control in Structures: Applications of Fracture Mechanics. 3rd ed. ASTM International. https://doi.org/10.1520/MNL41-3RD-EB

[20] Pereira LS, Donato GHB, Neto MM (2023) Assessment of the Von Mises Stresses and Stress Triaxiality in Notches Using Modified Tensile Specimens. Materials Research 26(1): 1–8. https://doi.org/10.1590/1980-5373-MR-2022-0572

[21] Simão LG (2024) Determination of the K_{Ic} of a 7075 T6 Aluminum Alloy Using the Notched Cylinder Model Associated With a Mechanical-Metallurgical Hybrid Study. PhD Thesis (in Portuguese). Northern Fluminense State University, Brazil, 244p;

[22] Peng Z, Zhao H, Li X, Yuan L, Zhu T (2023) Ductile fracture of X80 pipeline steel over a wide range of stress triaxialities and Lode angles. Engineering Fracture Mechanics 289: 109470; 10.1016/j.engfracmech.2023.109470

[23] Wang J, Jia H, Wu M, Pi A, Huang F, Wang Z, Hao F (2025) Coupling effect of stress triaxiality and Lode angle over a wide range on the ductile fracture behavior and mechanism of high-strength steel 30CrMnSiNi2MoVE. Engineering Fracture Mechanics 325: 111302; 10.1016/j.engfracmech.2025.111302

[24] Haythornthwaite DR (1961) Range of Yield Condition in Ideal Plasticity. Transactions of the American Society of Civil Engineers 127;

[25] Mohr D, Marcadet SJ (2015) Micromechanically-motivated phenomenological Hosford-Coulomb model for predicting ductile fracture of

metal sheets at low stress triaxialities. International Journal of Solids and Structures 67: 40-55;
10.1016/j.ijsolstr.2015.02.024

[26] Song Y, Guo Y, Liu G, Han J, Wang S, He W, Zhu S (2024) An enhanced Hosford–Coulomb fracture model for predicting ductile fracture under a wide range of stress states. Engineering Fracture Mechanics 312: 110635;
10.1016/j.engfracmech.2024.110635

[27] Park J, Kweon S, Park K (2024) Gurson-Cohesive modeling (GCM) for 3D ductile fracture simulation. International Journal of Plasticity 175: 103914;
https://doi.org/10.1016/j.ijplas.2024.103914

[28] Shen F, Sparrer Y, Rao J, Könemann M, Münstermann S, Lian J (2024) A forming limit framework accounting for various failure mechanisms: Localization, ductile and cleavage fracture. International Journal of Plasticity 175: 103921;
https://doi.org/10.1016/j.ijplas.2024.103921

[29] Chen A, Zhang P, Chen B, Li Y, Xing J (2023) A new ductile fracture model for Q460C high-strength structural steel under monotonic loading: Experimental and numerical investigation. Engineering Fracture Mechanics 288: 109358;
10.1016/j.engfracmech.2023.109358

[30] Tada H, Irwin G, Paris P (2000) The Stress Analysis of Cracks Handbook. 3rd ed. ASME Press, New York;
[31] Simão LG, Carvalho EA (2023) K_{Ic} Determination of a 7075 T6 Aluminum Alloy by Critical Distances Theory and LEFM. Materials Research 26: 1-8;
https://doi.org/10.1590/1980-5373-MR-2023-0056

[32] The European Union (2009) Eurocode 9: Design of aluminium structures, English Version. EN 1999-1-1 :2007+A1. Brussels, Belgium;

[33] Anderson TL (2005) Fracture Mechanics: Fundamentals e Applications. 3rd ed. Taylor & Francis Group, Boca Raton;

[34] Gurson AL (1977) Continuum theory of ductile rupture by void nucleation and growth: Part I—Yield criteria and flow rules for porous ductile media. Journal of Engineering Materials and Technology 99(1): 2-15; https://doi.org/10.1115/1.3443401

[35] Tvergaard V, Needleman A (1984) Analysis of the cup-cone fracture in a round tensile bar. Acta Metallurgica 32(1): 157-169; https://doi.org/10.1016/0001-6160(84)90213-X

[36] Chen DH, Chen L (2018) The Admissible Range of notch Radius for Applying the Singular Stress Field to Its Fracture Analysis. Engineering Fracture Mechanics 202: 202-213; 10.1016/j.engfracmech.2018.09.005

[37] American Society for Testing and Materials (2016) Standard Test Methods for Tension Testing of Metallic Materials: ASTM E8, United States;

[38] Saeidi N, Ekrami A (2009) Comparison of mechanical properties of martensite/ferrite and bainite/ferrite dual phase 4340 steels. Materials Science and Engineering A 523: 125-129; https://doi.org/10.1016/j.msea.2009.06.057

[39] Creager M, Paris PC (1967) Elastic field equations for blunt cracks with reference to stress corrosion cracking. International Journal of Fracture Mechanics 3(4): 247-252.

Appendix A

A1. Estimation of η_{max} in a CTS Type Test Specimen – Crack Case

The stress field in the vicinity of a crack of constant length along the thickness of the body acting on the resistant section has the following stress components:

$$\sigma_x = \frac{K_I}{\sqrt{2\pi r}}\left(cos\,\frac{\theta}{2}\right)\left[1 - sin\,\frac{\theta}{2}sin\,\frac{3\theta}{2}\right] \quad (A1)$$

$$\sigma_y = \frac{K_I}{\sqrt{2\pi r}}\left(cos\,\frac{\theta}{2}\right)\left[1 + sin\,\frac{\theta}{2}sin\,\frac{3\theta}{2}\right] \quad (A2)$$

$$\tau_{xy} = \frac{K_I}{\sqrt{2\pi r}}cos\left(\frac{\theta}{2}\right)sin\left(\frac{\theta}{2}\right)cos\left(\frac{3\theta}{2}\right) \quad (A3)$$

Since the region of interest is in the crack plane, where Θ = 0°, and r is in the vicinity of the crack (i.e., r ≠ 0), we have that:

$$\sigma_x = \sigma_y = \frac{K_I}{\sqrt{2\pi r}} \quad (A4)$$

$$\tau_{xy} = 0 \quad (A5)$$

The condition of interest is the Plane Strain State, where $\varepsilon_z = 0$. This gives rise to the third stress component, σ_z:

$$\sigma_z = v\left(\sigma_x + \sigma_y\right) \quad (A6)$$

Applying expression (A4) to (A6), we have:

$$\sigma_z = v\left(\frac{K_I}{\sqrt{2\pi r}} + \frac{K_I}{\sqrt{2\pi r}}\right) = 2v\left(\frac{K_I}{\sqrt{2\pi r}}\right) \quad (A7)$$

On the other hand, the calculation of the triaxiality index, in the region near the tip of the crack, is given by the expression:

$$\eta = \frac{\sigma_m}{\sigma_{vM}} \quad \text{(A8)}$$

Where σ_m is the average stress and σ_{vM} is the von Mises stress, as described below:

$$\sigma_m = \frac{\sigma_1+\sigma_2+\sigma_3}{3} \quad \text{(A9)}$$

$$\sigma_{vM} = \sqrt{\frac{1}{2}((\sigma_1-\sigma_2)^2+(\sigma_2-\sigma_3)^2+(\sigma_3-\sigma_1)^2)} \quad \text{(A10)}$$

Applying expressions (A4) and (A7) in (A9) and (A10), we have that:

$$\sigma_m = \frac{K_I}{\sqrt{2\pi r}}\frac{(2+2v)}{3} \quad \text{(A11)}$$

$$\sigma_{vM} = \frac{K_I}{\sqrt{2\pi r}}\sqrt{(1-4v+4v^2)} \quad \text{(A12)}$$

Applying (A11) and (A12) again in (A8), we get:

$$\eta_{max} = \frac{(2+2v)}{3\sqrt{(1-4v+4v^2)}} \quad \text{(A13)}$$

A2. Estimation of η_{max} in a CTS Type Test Specimen – Notch Case

The stress field in the vicinity of a notch of constant length along the thickness of the body acting on the resistant section and having a notch root radius, ρ, has the following stress components for mode I opening, according to Creager and Paris [39]:

$$\sigma_x = \frac{K_I}{\sqrt{2\pi r}}\left(cos\frac{\theta}{2}\right)\left[1-sin\frac{\theta}{2}sin\frac{3\theta}{2}\right]-\frac{K_I}{\sqrt{2\pi r}}\left(\frac{\rho}{2r}\right)cos\frac{3\theta}{2} \quad \text{(A14)}$$

$$\sigma_y = \frac{K_I}{\sqrt{2\pi r}}\left(cos\frac{\theta}{2}\right)\left[1+sin\frac{\theta}{2}sin\frac{3\theta}{2}\right]+\frac{K_I}{\sqrt{2\pi r}}\left(\frac{\rho}{2r}\right)cos\frac{3\theta}{2} \quad \text{(A15)}$$

$$\tau_{xy} = \frac{K_I}{\sqrt{2\pi r}} sin\frac{\theta}{2} cos\frac{\theta}{2} cos\frac{3\theta}{2} - \frac{K_I}{\sqrt{2\pi r}}\left(\frac{\rho}{2r}\right) sin\frac{3\theta}{2} \quad \text{(A16)}$$

Since the region of interest is in the crack plane, where Θ = 0°, and r is in the vicinity of the crack (i.e., r ≠ 0), we have that:

$$\sigma_x = \frac{K_I}{\sqrt{2\pi r}}\left(1 - \frac{\rho}{2r}\right) \quad \text{(A17)}$$

$$\sigma_y = \frac{K_I}{\sqrt{2\pi r}}\left(1 + \frac{\rho}{2r}\right) \quad \text{(A18)}$$

$$\tau_{xy} = 0 \quad \text{(A19)}$$

The condition of interest is the Deformation Plane State, where $\varepsilon_z = 0$. This gives rise to the third stress component, σ_z:

$$\sigma_z = v(\sigma_x + \sigma_y) \quad \text{(A20)}$$

Applying expression A17 and A18 in A20, we have:

$$\sigma_z = v\left(\frac{K_I}{\sqrt{2\pi r}} + \frac{K_I}{\sqrt{2\pi r}}\right) = 2v\left(\frac{K_I}{\sqrt{2\pi r}}\right) \quad \text{(A21)}$$

The "smoothing" of the notch (the term ρ/2r) affects σ_x and σ_y in opposite ways, and its effect on the sum is canceled out.

Applying expressions (A17), (A18), and (A21) in (A9) and (A10), we have:

$$\sigma_m = \frac{K_I}{\sqrt{2\pi r}} \frac{(2+2v)}{3} \quad \text{(A22)}$$

The average (hydrostatic) stress along the axis of symmetry (x) is independent of the notch root radius. It is identical to the average stress of Irwin's singular solution (for an acute crack).

And for von Mises:

$$\sigma_{vM} = \frac{K_I}{\sqrt{2\pi r}} \sqrt{\frac{3\rho^2}{4r^2} + (1-2v)^2} \quad \text{(A23)}$$

Again applying (A22) and (A23) in (A8), we get:

$$\eta_{max} = \frac{(2+2v)}{3\sqrt{\frac{3\rho^2}{4r^2} + (1-2v)^2}} \quad \text{(A24)}$$

The expression (A24) indicates that in the region near the notch root and in the plane of the resistant section, the maximum triaxiality intensity, expressed by η_{max}, is dependent on Poisson's ratio, the notch root radius (ρ), and the position (x). Expression (A24) produces results identical to (A13) up to the limit of R/ρ = 60. These values refer, again, to the case of CTS.